



## Synthesis, characterization and DNA binding studies of organoantimony(V) ferrocenyl benzoates

Faiza Asghar<sup>a</sup>, Amin Badshah<sup>a,\*</sup>, Afzal Shah<sup>a</sup>, Muhammad Khawar Rauf<sup>a</sup>, Muhammad Irshad Ali<sup>a</sup>, Muhammad Nawaz Tahir<sup>b</sup>, Erum Nosheen<sup>a</sup>, Zia-ur-Rehman<sup>a</sup>, Rumana Qureshi<sup>a</sup>

<sup>a</sup> Department of Chemistry, Quaid-i-Azam University, Islamabad 45320, Pakistan

<sup>b</sup> University of Sargodha, Department of Physics, Sargodha, Pakistan

### ARTICLE INFO

#### Article history:

Received 23 May 2012

Received in revised form

4 July 2012

Accepted 15 July 2012

#### Keywords:

Organoantimony(V) ferrocenyl benzoates

Single crystal XRD

Cyclic voltammetry

UV–Vis spectroscopy

Complex–DNA interaction

### ABSTRACT

Organoantimony(V) ferrocenyl benzoates (OFBs) [ $p$ -(C<sub>5</sub>H<sub>5</sub>FeC<sub>5</sub>H<sub>4</sub>)C<sub>6</sub>H<sub>4</sub>COO]<sub>2</sub>SbR<sub>3</sub> (R = C<sub>6</sub>H<sub>5</sub>,  $p$ -CH<sub>3</sub>C<sub>6</sub>H<sub>4</sub>) (**3**, **4**) and [ $m$ -(C<sub>5</sub>H<sub>5</sub>FeC<sub>5</sub>H<sub>4</sub>)C<sub>6</sub>H<sub>4</sub>COO]<sub>2</sub>SbR<sub>3</sub> (R =  $p$ -CH<sub>3</sub>C<sub>6</sub>H<sub>4</sub>) (**5**) were synthesized and characterized by FT-IR, <sup>1</sup>H and <sup>13</sup>C NMR, single crystal XRD and elemental analysis. The DNA interaction of the complexes (**3–5**) was investigated by UV–Vis spectroscopy and cyclic voltammetry (CV). The complex–DNA binding constant was found to vary in the sequence:  $K_2$  ( $4.80 \times 10^5$ ) >  $K_1$  ( $2.36 \times 10^4$ ) >  $K_3$  ( $1.87 \times 10^4$ ) >  $K_4$  ( $6.61 \times 10^3$ ) >  $K_5$  ( $6.58 \times 10^3$ ). The shift in peak potential, current and absorption maxima of OFBs in the presence of DNA revealed that CV coupled with UV–Vis spectroscopy could provide a convenient way to characterize complex–DNA interaction mechanism, a prerequisite for the design of new anticancer agents and understanding the molecular basis of their action.

© 2012 Elsevier B.V. All rights reserved.

### 1. Introduction

Synthesis, structural aspects and antitumor activities of ferrocenyl benzoate–antimony complexes have been the subject of intensive investigations [1–4]. Among the organometallic compounds, ferrocene has captured the utmost attention for conjugation with biomolecules due to its stability in aqueous media, large variety of derivatization, facile oxidation and the unique property of retaining simple one electron redox behavior after the introduction of substituents at the cyclopentadienyl rings [5–7]. Medicinal application of ferrocene is an active area of research and many reports have shown that ferrocenyl derivatives are endowed with interesting cytotoxic [8–10], antitumor [11,12], antifungal [13], antimalarial [14] and DNA-cleaving activities [15].

Antimony was first introduced into medicinal treatment in 16th century and gained a growing interest due to its emetic effect [16]. The organic derivatives of the element in both trivalent and pentavalent states are known which leads to many different classes of compounds that have various therapeutic and technological applications. The pentavalent antimonials became the first choice

of chemotherapy due to their efficient therapeutic index and 10-fold lower toxicity than trivalent analogues [17–19]. The major clinical use of organoantimonials is in the treatment of leishmaniasis. Some organoantimony derivatives such as antimony tartrate [20] and sodium stibogluconate [21,22] have been reported to exhibit significant anti-cancer and anti-viral activities as well.

Deoxyribonucleic acid, DNA, is a molecule of great biological significance since it contains all the genetic information for cellular function. The interaction of small molecules to DNA is gaining wide spread importance. This interaction may be summarized in three ways: (a) electrostatic, (b) groove binding and (c) intercalation [23,24]. A variety of analytical techniques have been used to study the drug–DNA interactions such as luminescence [25], fluorescence [26], UV–visible spectroscopy [27], and voltammetric methods [28–30]. But the electrochemical methods are most widely used due to their advantages like high sensitivity, cost effectivity, more reliability and fast detection ability. UV–Vis spectroscopic technique is also best suited to ferrocenes owing to their intense colors. In this paper, we have synthesized organoantimony derivatives of  $m$ -ferrocenylbenzoic acid and  $p$ -ferrocenylbenzoic acid (**3–5**), which contain three active centers, namely the organoantimony (V) moiety and two ferrocenyl carboxylate groups. The synthesis and characterization of compound (**5**) bis( $p$ -ferrocenylbenzoato)tri( $p$ -tolyl) antimony(V) have already been reported by Yu et al. [1], but crystallographic and electrochemical studies have not yet been reported.

\* Corresponding author. Tel.: +92 5190642131; fax: +92 5190642241.

E-mail addresses: [aminbadshah@yahoo.com](mailto:aminbadshah@yahoo.com) (A. Badshah), [mkhawarrauf@yahoo.co.uk](mailto:mkhawarrauf@yahoo.co.uk) (M.K. Rauf).

The main objective of the present work is to investigate the DNA binding potential of these compounds by spectrophotometric and electrochemical techniques. In addition we are interested in studying the tunable redox and spectroscopic properties of the DNA binding ferrocenes for the provision of useful insights about the design of anticancer drugs and understanding of unexplored pathways by which such compounds exert their biochemical action.

## 2. Experimental

### 2.1. Materials and methods

All the manipulations were carried out under the specified conditions of temperature. Solvents were distilled from the drying agents and degassed before use.

NMR spectra were recorded on a Bruker ARX, 300 MHz spectrometer.  $^1\text{H}$  NMR (300 MHz): internal standard solvent  $\text{CDCl}_3$  (7.28 ppm from TMS); internal standard TMS;  $^{13}\text{C}$  NMR (75.47 MHz): internal standard solvent  $\text{CDCl}_3$  (77.0 ppm from TMS); internal standard TMS; the splitting of proton resonances in the reported  $^1\text{H}$  NMR spectra are defined as s = singlet, d = doublet, t = triplet, q = quartet and m = complex pattern; coupling constants are reported in Hz. FT-IR spectra were recorded as KBr pellets on a Bio-Rad Excalibur FT-IR Model FTS 3000 MX (400–4000  $\text{cm}^{-1}$ ) and on ATR with Perkin Elmer System 2000 (200–500  $\text{cm}^{-1}$ ). The elemental analyses were performed using a LECO-932 CHNS analyzer. The melting points were determined on a Bio Cote SMP10- UK and are uncorrected. All solvents were purified by distillation, dried under an atmosphere of nitrogen and stored over molecular sieves 4 Å.

Commercial salmon sperm DNA was gifted by Prof. Dr. Muhammad Siddiq. Its stock solution of  $2.50 \times 10^{-4}$  M was prepared in doubly distilled water and stored at 4 °C. The concentration of the stock solution was determined from UV absorbance at 260 nm using a molar extinction coefficient ( $\epsilon$ ) of  $6600 \text{ M}^{-1} \text{ cm}^{-1}$ . A ratio of absorbance at 260 and 280 nm of ( $A_{260}/A_{280}$ ) > 1.8 indicated protein free DNA.

Cyclic voltammetric experiments were performed using  $\mu\text{Autolab}$  running with GPES 4.9 software, Eco-Chemie, The Netherlands. A glassy carbon (GC) ( $A = 0.07 \text{ cm}^2$ ) was used as working electrode, a Pt wire served as counter electrode and a saturated calomel electrode (SCE) was employed as the reference. Before each experiment the surface of GCE was polished with alumina powder followed by thorough rinsing with distilled water. Electrochemical grade tetrabutylammonium fluoroborate (TBAFB) was used as supporting electrolyte. All the voltammetric experiments were conducted in a high purity nitrogen (99.995%) atmosphere at room temperature ( $25 \pm 1$  °C).

Absorption spectra were recorded on Shimadzu 1601 spectrophotometer. First the spectra of the analytes were recorded in the absence of DNA and then in the presence of different concentration of DNA by keeping the volume and concentration of the compound constant. Equal amount of DNA was added to both reference and sample cells in order to avoid the appearance of its peak at about 260 nm where ferrocene also absorbs.

Chemicals ferrocene, *m*-nitroaniline, *p*-nitroaniline, sodium nitrite, antimony(III) chloride, bromobenzene, *p*-bromotoluene and solvents were purchased from Sigma–Aldrich and used after purification, where needed.

### 2.2. General procedure for the synthesis of organo-antimony (V) ferrocenyl benzoates (3–5)

The organo-antimony (V) ferrocenyl benzoates have been synthesized according to a reported method with some

modifications [1]. To a double neck round bottom flask sodium salts of *m*-ferrocenyl benzoic acid (0.01 mol) or *p*-ferrocenyl benzoic acid (0.01 mol) was added in 50 ml of chloroform and the reaction mixture was allowed to stir for about an hour. Then (0.005 mol) organo-antimony(V) was added and the suspension was refluxed for 5–6 h. The progress of the reaction mixture was maintained by TLC (chloroform/*n*-hexane 40:60). Precipitates of the salt formed were filtered off and the filtrate was evaporated under vacuum. Residue was dissolved in dichloromethane/chloroform and kept for crystallization (Scheme 1). The synthesis and characterization of compound (5) bis (*p*-ferrocenylbenzoato)tri(*p*-tolyl)antimony(V) have already been reported by Yu et al. [1], but crystallographic and electrochemical studies have not yet been reported.

#### 2.2.1. Bis (*m*-ferrocenylbenzoato)triphenylantimony(V) (3)

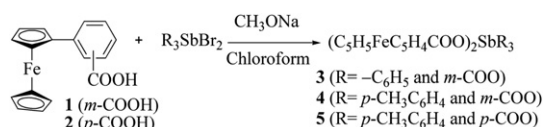
Quantities used were 3.10 g (0.01 mol) *m*-ferrocenyl benzoic acid and 2.56 g (0.005 mol) organo-antimony(V); Yield 79%; Brown solid; m.p. 190–192 °C; FT-IR (KBr,  $\text{cm}^{-1}$ ) 3021 (C–H<sub>aromatic</sub>), 1651 (C=O), 1600 (C=C), 534–582 (Sb–O), 482 (Fe–Cp), 443–461 (Sb–C);  $^1\text{H}$  NMR (300 MHz,  $\text{CDCl}_3$ , 25 °C)  $\delta$  4.03 (s, 10H, C<sub>5</sub>H<sub>5</sub>), 4.33 (t, 4H, C<sub>5</sub>H<sub>4</sub>,  $J = 1.8$  Hz), 4.65 (t, 4H, C<sub>5</sub>H<sub>4</sub>,  $^3J = 1.8$  Hz), 7.32 (d, 2H, ArH,  $^3J = 7.8$  Hz), 7.53–7.61 (m, 11H, ArH), 7.81 (d, 2H, ArH,  $^3J = 7.8$  Hz), 8.04 (s, 2H, ArH), 8.20 (dd, 6H, ArH,  $^3J = 7.5$  Hz,  $^4J = 4.2$  Hz);  $^{13}\text{C}$  NMR (75.47 MHz,  $\text{CDCl}_3$ , 25 °C)  $\delta$  66.7 (4C, meta on C<sub>5</sub>H<sub>4</sub>), 69.1 (4C, ortho on C<sub>5</sub>H<sub>4</sub>), 69.6 (10C, C<sub>5</sub>H<sub>5</sub>), 84.7 (2C, C<sub>5</sub>H<sub>4</sub>), 127.4 (2C, Ar), 127.6 (2C, Ar), 128.1 (2C, Ar), 129.5 (6C, Ar), 131.3 (3C, Ar), 132.8 (2C, Ar), 133.9 (6C, Ar), 137.9 (2C, Ar), 139.4 (3C, ipso-C, Ar), 170.1 (2C, C=O); Anal. Calcd. for C<sub>52</sub>H<sub>41</sub>Fe<sub>2</sub>O<sub>4</sub>Sb: C, 64.83; H, 4.29; Found: C, 64.78; H, 4.26.

#### 2.2.2. Bis (*m*-ferrocenylbenzoato)tri(*p*-tolyl)antimony(V) (4)

Quantities used were 3.10 g (0.01 mol) *m*-ferrocenyl benzoic acid and 2.77 g (0.005 mol) organo-antimony(V); Yield 82%; Brown solid; m.p. 184–185 °C; FT-IR (KBr,  $\text{cm}^{-1}$ ) 3065–3092 (C–H<sub>aromatic</sub>), 2856–2922 (C–H<sub>aliphatic</sub>), 1643 (C=O), 1598 (C=C), 535–574 (Sb–O), 481–491 (Fe–Cp), 447–456 (Sb–C);  $^1\text{H}$  NMR (300 MHz,  $\text{CDCl}_3$ , 25 °C)  $\delta$  2.41 (s, 9H, –CH<sub>3</sub>), 4.04 (s, 10H, C<sub>5</sub>H<sub>5</sub>), 4.34 (t, 4H, meta on C<sub>5</sub>H<sub>4</sub>,  $J = 1.8$  Hz), 4.66 (t, 4H, ortho on C<sub>5</sub>H<sub>4</sub>,  $J = 1.8$  Hz), 7.21–7.33 (m, 2H, ArH), 7.36 (d, 2H, ArH,  $^3J = 8.1$  Hz), 7.59 (d, 2H, ArH,  $^3J = 7.8$  Hz), 7.81 (d, 2H, ArH,  $^3J = 7.8$  Hz), 8.05 (s, 2H, ArH), 8.08 (d, 6H, ArH,  $^3J = 8.1$  Hz);  $^{13}\text{C}$  NMR (75.47 MHz,  $\text{CDCl}_3$ , 25 °C)  $\delta$  21.6 (3C, –CH<sub>3</sub>), 66.7 (4C, meta on C<sub>5</sub>H<sub>4</sub>), 69.0 (4C, ortho on C<sub>5</sub>H<sub>4</sub>), 69.6 (10C, C<sub>5</sub>H<sub>5</sub>), 84.8 (2C, C<sub>5</sub>H<sub>4</sub>), 128.0 (3C, Ar), 128.3 (2C, Ar), 129.1 (2C, Ar), 129.5 (2C, Ar), 130.3 (6C, Ar), 133.2 (2C, Ar), 133.8 (6C, Ar), 134.2 (2C, Ar), 139.3 (2C, Ar), 141.5 (3C, ipso-C, Ar), 169.9 (2C, C=O); Anal. Calcd. for C<sub>55</sub>H<sub>47</sub>Fe<sub>2</sub>O<sub>4</sub>Sb: C, 65.70; H, 4.71; Found: C, 65.63; H, 4.69.

#### 2.2.3. Bis (*p*-ferrocenylbenzoato)tri(*p*-tolyl)antimony(V) chloroform solvate (5) [1]

Quantities used were 3.10 g (0.01 mol) *p*-ferrocenyl benzoic acid and 2.77 g (0.005 mol) organo-antimony(V); Yield 84%; Orange solid; m.p. 205 °C (dec); FT-IR (KBr,  $\text{cm}^{-1}$ ) 3059 (C–H<sub>aromatic</sub>), 2923–2852 (C–H<sub>aliphatic</sub>), 1625 (C=O), 1605 (C=C), 566 (Sb–O), 476 (Fe–Cp), 456 (Sb–C);  $^1\text{H}$  NMR (300 MHz,  $\text{CDCl}_3$ , 25 °C)  $\delta$  2.40 (s, 9H, –CH<sub>3</sub>), 4.04 (s, 10H, C<sub>5</sub>H<sub>5</sub>), 4.37 (s, 4H, meta on C<sub>5</sub>H<sub>4</sub>), 4.68 (s, 4H, ortho on C<sub>5</sub>H<sub>4</sub>), 7.34 (d, 6H, ArH,  $^3J = 8.1$  Hz), 7.45 (d, 4H, ArH,  $^3J = 8.4$  Hz), 7.88 (d, 4H, ArH,  $^3J = 8.4$  Hz), 8.05 (d, 6H, ArH,



Scheme 1. Synthesis of organoantimony(V) ferrocenyl benzoates (3–5).

$^3J = 8.1$  Hz);  $^{13}\text{C}$  NMR (75.47 MHz,  $\text{CDCl}_3$ , 25 °C)  $\delta$  21.6 (3C,  $-\text{CH}_3$ ), 66.8 (4C, meta on  $\text{C}_5\text{H}_4$ ), 67.9 (4C, ortho on  $\text{C}_5\text{H}_4$ ), 69.5 (10C,  $\text{C}_5\text{H}_5$ ), 83.9 (2C,  $\text{C}_5\text{H}_4$ ), 125.4 (4C, Ar), 130.0 (4C, Ar), 130.2 (6C, Ar), 130.4 (2C, Ar), 133.8 (6C, Ar), 134.5 (3C, Ar), 141.3 (2C, Ar), 143.7 (3C, *ipso*-C, Ar), 169.8 (2C, C=O); Anal. Calcd. for  $\text{C}_{56}\text{H}_{48}\text{Cl}_3\text{Fe}_2\text{O}_4\text{Sb}$ : C, 59.80; H, 4.30; Found: C, 59.76; H, 4.28.

### 2.3. Data collection and structural refinement of 5

Crystals of **5** was grown by the slow evaporation method in toluene/chloroform (0.25:1). The reddish crystals were mounted in a random orientation on a glass fiber and aligned on a Bruker kappa APEXII CCD diffractometer using graphite-monochromated Mo- $K\alpha$  radiation ( $\lambda = 0.71073$  Å). Data collection used  $\omega$  scans, and a multi-scan absorption correction was applied. The structure was solved by using SHELXS97 program [31]. The hydrogen atoms were generated by geometrical considerations. Final refinement on  $F^2$  carried out by full matrix least-squares techniques using SHELXL-97. The disordered cyclopentadienyl's were refined in two groups as regular pentagons having equal occupancy ratio. The disordered C atoms were refined as anisotropic with equal thermal parameters in groups. The Cl atoms of the chloroform were refined over three positions with occupancy ratio 0.60:0.20:0.20 and refined as anisotropic with similar thermal parameters. Table 1 (suppl) summarizes the crystal data and refinement values.

## 3. Results and discussion

### 3.1. Chemistry

Two derivatives of ferrocene carboxylic acids (**1**, **2**), *m*-ferrocenyl benzoic acid (**1**) and *p*-ferrocenyl benzoic acid (**2**) were synthesized by using a standard method [32]. By reacting these ligands with organoantimony(V) complexes, a series of hetero-bimetallic complexes (**3–5**), namely: bis(*m*-ferrocenylbenzoato)triphenylantimony(V) (**3**) bis(*m*-ferrocenylbenzoato)tri(*p*-tolyl)antimony(V) (**4**) and bis(*p*-ferrocenylbenzoato)tri(*p*-tolyl)antimony(V) (**5**), were also synthesized (Scheme 1). The purity of the ligands and complexes was checked by TLC with Merck Kieselgel GF 254 Plates, elemental analysis,  $^1\text{H}$ - and  $^{13}\text{C}$ -NMR (Bruker ARX, 300 MHz spectrometer).

### 3.2. Spectroscopic studies

The ferrocene carboxylic acids and their antimony(V) complexes (**3–5**) were synthesized in good yield, which were characterized by different analytical techniques. The FT-IR spectra of the compounds have been recorded in the range of 4000–400  $\text{cm}^{-1}$ . In the spectra of all the compounds no characteristic band was observed in the range of 3500–3300  $\text{cm}^{-1}$  due to  $\nu(\text{OH})$ , indicating that deprotonation and coordination of antimony metal with carboxylate group have occurred as was expected. The absorption bands for the carbonyl groups are observed in the region 1651–1625  $\text{cm}^{-1}$ . In addition, the absorption frequencies due to Sb–O bond are observed at 532–582  $\text{cm}^{-1}$ , while that for Sb–C bond appears at 443–461  $\text{cm}^{-1}$ .

The  $^1\text{H}$  NMR spectra of complexes (**3–5**) show that the unsubstituted cyclopentadienyl ( $\eta^5\text{-C}_5\text{H}_5$ ) rings give a singlet of high intensity at  $\delta$  4.0. In the case of substituted ( $\eta^5\text{-C}_5\text{H}_4$ ) ring the *ortho* protons appear in the region  $\delta$  4.65–4.69 while the *meta* protons occur in the range of  $\delta$  4.33–4.37. The splitting pattern for the *meta* derivatives (**3**, **4**) consisted of a singlet, two doublets and a multiplet that each integrated for two protons. For the *para* substituted derivative (**5**) the pattern observed was two doublets that each integrate for four protons. The phenyl groups attached to antimony

(**3**) gives a doublet of a doublet for six protons and a multiplet integrating for nine protons. The *p*-tolyl groups attached to antimony (**4**, **5**) appear as two doublets that each integrate for six protons.

In the  $^{13}\text{C}$ -NMR spectra of compounds (**3–5**) the carbonyl carbon atoms appear in the narrow range of  $\delta$  169.8–170.2. The ferrocenyl carbon atoms show signals in the region  $\delta$  66.7–84.8. The *ipso*-carbon of the ( $\eta^5\text{-C}_5\text{H}_4$ ) ring appears in the range of  $\delta$  83.9–84.8. The unsubstituted cyclopentadienyl ( $\eta^5\text{-C}_5\text{H}_5$ ) ring gives an intense peak at  $\delta$  69.5–69.8, while for substituted cyclopentadienyl ( $\eta^5\text{-C}_5\text{H}_4$ ) ring the *ortho* and *meta* carbon atoms have chemical shifts in the region  $\delta$  66.7–69.5. In the case of *meta* derivatives (**3**, **4**) all the carbon atoms of the aromatic ring are non-equivalent, therefore six signals are observed. While the *para* substituted derivative (**5**) display four signals.

All the synthesized complexes were characterized by elemental analysis using a CHNS analyzer. The results indicated that the ligand to metal ratio in complexes is 1:2 which was further confirmed by the crystal structure of the complex **5**.

### 3.3. Structural studies

Product **5** grew in a monoclinic system with the  $P2_1/n$  space group. The important geometric parameters are given in Table 1. The complex adopts an approximate trigonal bipyramidal Sb coordination environment with unidentate carboxylate ligands in the axial positions [Sb–O: 2.114(3)–2.143(3) Å, O–Sb–O: 175.30(14)°] at *trans* orientation with respect to ferrocenyl moiety. The three *p*-tolyl groups are in the equatorial plane and show a distortion towards square-based pyramidal with a widening of one of the trigonal angle [C–Sb–C: 143.0(2)°]. The cyclopentadienyl ring was coplanar with the adjacent phenyl ring [dihedral angles 5.08 (18)]. The cyclopentadienyl ring A (C29–C33), phenyl rings B (C23–C28) and C (C40–C45) are planar with *r.m.s.* deviations of 0.0011, 0.0106 and 0.0037 Å, respectively. The dihedral angle between A/B is 5.08 (18)° which shows that central phenyl ring is almost planar with attached cyclopentadienyl. The dihedral angle between B/C is 11.07 (14)°. Three cyclopentadienyl rings of ferrocene are disordered over two set of sites with equal occupancy ratios. Selected bond lengths and bond angles are summarized in Table 1 (Fig. 1).

### 3.4. Cyclic voltammetry of OFBs interacting with DNA

The CV of 1 mM OFB (**3**) in the absence and presence of 2–20  $\mu\text{M}$  DNA at polished GCE has been shown in Fig. 2. The voltammogram without DNA featured a couple of robust peaks in the potential range of 0.0–1.5 V. The anodic and cathodic peaks appeared at 0.96 and 0.84 V versus SCE, while simple ferrocene was found to oxidize at 0.52 V under the same conditions. The difference of 0.44 V in the

**Table 1**  
Selected bond lengths (Å) and angles (°) for **5**.

Sb(1)–C(1)	2.113(5)	C(1)–Sb(1)–C15	107.32(19)
Sb(1)–C(15)	2.106(5)	C(1)–Sb(1)–O(3)	90.16(15)
Sb(1)–O(3)	2.114(3)	C(15)–Sb(1)–O(3)	87.10(16)
Sb(1)–C(8)	2.114(4)	C(1)–Sb(1)–C(8)	143.0(2)
Sb(1)–O(2)	2.143(3)	C15–Sb(1)–C(8)	109.7(2)
Fe(2)–C(33)	2.018(5)	O3–Sb(1)–C(8)	90.48(15)
Fe(2)–C(32)	2.028(5)	C(1)–Sb(1)–O(2)	91.67(15)
Fe(2)–C(31)	2.036(6)	C(15)–Sb(1)–O(2)	88.22(17)
Fe(2)–C(29)	2.038(4)	O(3)–Sb(1)–O(2)	175.30(14)
Fe(2)–C(30)	2.044(6)	C(8)–Sb(1)–O(2)	90.68(15)
O(1)–C(22)	1.225(7)	C(33)–Fe(2)–C(32)	40.4(2)
O(4)–C(39)	1.217(7)	C(33)–Fe(2)–C(31)	67.8(2)

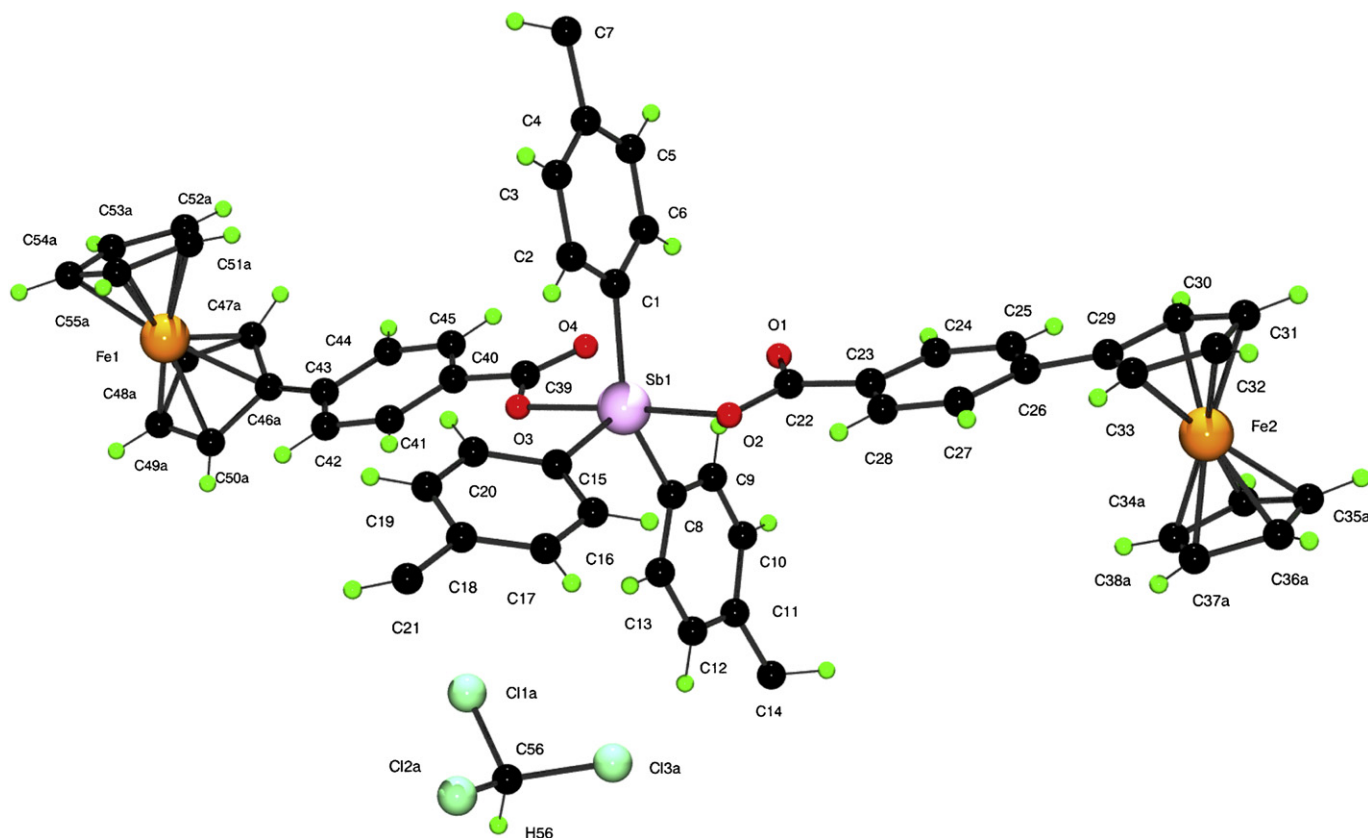


**Fig. 1.** Molecular diagram of **5** with non-hydrogen atoms represented by 30% probability boundary spheres and hydrogen atoms as spheres of arbitrary size. The  $\text{CHCl}_3$  solvent in the lattice has also been shown.

oxidation potentials of **3** and ferrocene is attributed to the electron withdrawing effect of benzoate group attached to the cyclopentadienyl ring of ferrocene, which causes its oxidation difficult. The electrochemical signal at 0.96 V reflects the oxidation of the ferrocenyl group of **3** to ferrocenium state, which gets reduced to its neutral form upon scan reversal. The anodic and cathodic peak current ratio ( $I_{pa}/I_{pc}$ ) of **1** is suggestive of reversible electrochemical process. In the presence of increasing concentration (2–20  $\mu\text{M}$ ) of DNA, the oxidation and reduction

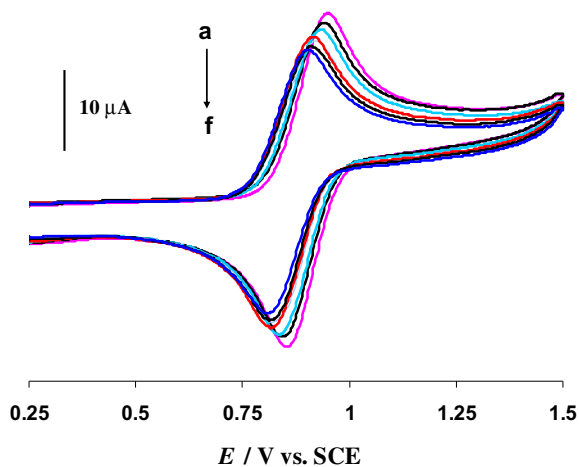


**Fig. 2.** CVs of 1 mM **3** in the (a) absence and presence of (b) 2, (c) 8 (d) 12, (e) 16 and (f) 20  $\mu\text{M}$  DNA in 10% aqueous ethanol (10%  $\text{H}_2\text{O}$ :90% ethanol),  $v$ : 100  $\text{mVs}^{-1}$ , supporting electrolyte: 0.1 M TBAFB.

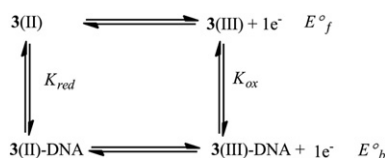
peak potentials of **3** shifted cathodically with the decrease in peak currents. The substantial diminution in peak currents is attributed to the formation of slowly diffusing **3**-DNA supramolecular complex due to which the concentration of the free drug (mainly responsible for the transfer of current) is lowered.

The DNA binding mode of a drug can be judged from the variation in formal potential. In general, positive shift in formal potential is observed for intercalation of the drug into the double helical structure of DNA [33], while negative shift is related to electrostatic interaction of cationic drug with anionic phosphate of DNA backbone [34]. So the obvious negative peak potential shift (cathodic shift) in the CV behavior of **3** is related to the electrostatic interaction of its positively charged ferrocenium state with the negatively charged oxygen of DNA. Like **3** the CVs of **4** and **5** (see Fig. 1 of Supplementary material) indicated the dominance of electrostatic interaction with DNA. Such an interaction is expected to induce perturbation in the normal functioning of DNA which could presumably culminate in the damage of its replication machinery and ultimate death of cancerous cell. The peak potential shift in the cathodic direction further indicates that Fe (II) of **3** is easier to oxidize in the presence of deoxyribonucleic acid because its oxidized form is more strongly bound to DNA. For such a system, where both forms of the drug interact with DNA, Scheme 2 can be applied [35].

Based upon the process discussed in Scheme 2, the following equation is obtained [36]

$$E_b^{\circ} - E_f^{\circ} = 0.059 \log(K_{\text{red}}/K_{\text{ox}}) \quad (1)$$

where  $E_f^{\circ}$  and  $E_b^{\circ}$  are the formal potentials of **3** (II)/**3** (III) couple in the free and bound forms respectively.



**Scheme 2.** General redox process of the free and DNA bound **3**.

For a shift of 40 mV caused by 1 mM **3** in the presence of 20  $\mu\text{M}$  DNA (Fig. 2) a ratio of  $K_{\text{red}}/K_{\text{ox}}$  was calculated as 0.21, which indicates 4.76 times stronger interaction of the oxidized form of the drug than the reduced form.

The CVs of **1** and **2** showed a dramatically different behavior in the presence of DNA. An increase in peak current of **1** along with cathodic peak potential shift was noticed (Fig. 3A) which may be related to the interaction of **1** with DNA in such a manner as to cause exposition of its nitrogenous bases. As DNA bases have been reported to oxidize in this region so their oxidation may have contribution in peak current elevation. In contrast to other ferrocene derivatives, the cathodic peak potential of **2** registered anodic shift along with peak current decay in the presence of DNA (Fig. 3B). Such CV characteristics can be related to the intercalation of the planar part of **2** into the stacked base pair pockets of deoxyribonucleic acid.

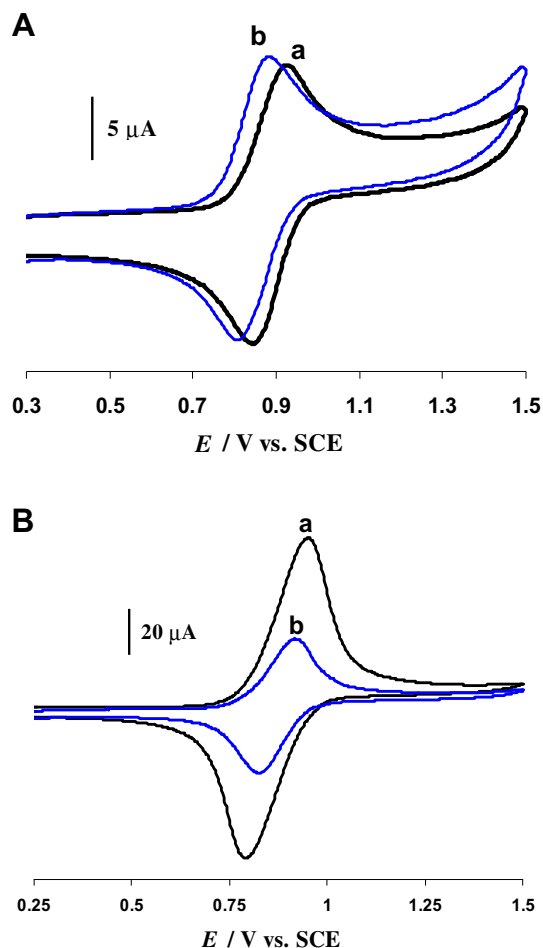


**Fig. 3.** CVs of 1 mM (A) **1** and (B) **2** in the (a) absence and (b) presence of 12  $\mu\text{M}$  DNA at 100 mV/s.

The interaction of **3** with DNA can be described by the following equation:



An equation for amperometric titrations can be deduced as [37,38],

$$\log(1/[\text{DNA}]) = \log K + \log(I/I_0 - I) \quad (3)$$

where  $K$  is the binding constant,  $I_0$  and  $I$  are the peak currents of the drug in the absence and presence of DNA respectively.

The decrease in peak current of **3** in the presence of increasing concentration of DNA was utilized for the evaluation of binding constant. The plot of  $\log(1/[\text{DNA}])$  versus  $\log(I/I_0 - I)$  (Fig. 4) yielded  $K = 1.87 \times 10^4 \text{ M}^{-1}$ , which is greater than the binding constant ( $K = 3.85 \times 10^3 \text{ M}^{-1}$ ) of a reported ferrocene based compound, *p*-nitrophenyl ferrocene [39].

The binding constants of **1**, **2**, **4** and **5** were also calculated according to Eq. (3).

The binding constant varied in the sequence:  $K_2 (4.80 \times 10^5) > K_1 (2.36 \times 10^4) > K_3 (1.87 \times 10^4) > K_4 (6.61 \times 10^3) > K_5 (6.58 \times 10^3)$ . The greater DNA binding affinity of **2** can be related to the mixed binding mode including electrostatic interaction (as verified by the negative shift of anodic peak in Fig. 3) of the iron of ferrocenyl group with anionic phosphate backbone of DNA and intercalation (as evidenced by the positive shift of cathodic peak potential) of the planar benzoate moiety into the base pair pockets of DNA. The comparatively high  $K$  value of **2** indicates its effectiveness as potential anticancer drug. The lower  $K$  value of **5** than **2** can be attributed to the presence of two ferrocenyl groups that block the planar moiety to intercalate. The same attribution is responsible for the lower  $K$  values of **3** and **4** than **1**.

The diffusion coefficients of the free and DNA bound ferrocene derivatives were determined by using Randles–Sevcik equation

$$I_{\text{pa}} = 2.69 \times 10^5 n^{3/2} ACD^{1/2} \nu^{1/2} \quad (4)$$

where  $I_{\text{pa}}$  is the anodic peak current in amperes,  $n$  is the number of electrons transferred during oxidation,  $A$  is the geometric area of the electrode in  $\text{cm}^2$ ,  $D$  is the diffusion coefficient in  $\text{cm}^2 \text{ s}^{-1}$ ,  $C$  is the bulk concentration of the reductant in  $\text{mol cm}^{-3}$  and  $\nu$  is the scan rate in  $\text{V s}^{-1}$  [40].

The results revealed that the values of diffusion coefficient of the DNA-bound ferrocenes are lower as compared to free ferrocenes due to the formation of slowly diffusing heavy drug-DNA adducts. The values of diffusion coefficient varying in the sequence:  $D_2 (9.93 \times 10^{-5}) > D_3 (9.94 \times 10^{-6}) > D_4 (6.41 \times 10^{-6}) > D_1 (2.44 \times 10^{-6}) > D_5 (1.10 \times 10^{-7})$  are comparable with other

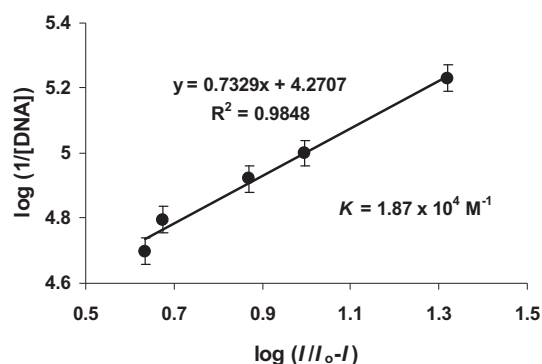


**Fig. 4.** Plot of  $\log(1/[\text{DNA}])$  vs.  $\log(I/I_0 - I)$  for the determination of **3**-DNA binding constant.

ferrocene derivatives reported in literature [41–43]. The relatively high  $D$  value of **2** may be due to its smaller molecular mass and more electron deficient iron due to better electron withdrawing ability of benzoate (attached at *para* position) from ferrocenyl group. The greater  $D$  value of **3** than **4** and **5** support the idea that molecules with smaller molecular mass diffuse quickly to the electrode surface. Generally, drugs interacting with DNA by intercalative mode have an order of magnitude lower  $D$  than their free forms while a slight decrease is observed for electrostatically interacting drugs. Based upon this criterion, all the ferrocene derivatives except **2** are suggested to interact with DNA via electrostatic interaction as the dominant mode. The comparatively larger difference in the  $D$  values of free and DNA bound **2** is attributed to the involvement of intercalation. The CVs of **5** and the plot between  $I_{pa}$  and  $\nu^{1/2}$  have been shown in supplementary materials as Fig. 3. The linearity of the plot indicates that the electrochemical process is diffusion controlled [44].

### 3.5. Electronic absorption spectroscopy of OFBs interacting with DNA

The UV–Vis spectra of 45  $\mu\text{M}$  **4** and **5** have been depicted in Fig. 5. Compound **5** registered five peaks at 234, 259, 296, 364 and 460 nm. The peak at 234 nm can be attributed to  $\pi \rightarrow \pi^*$  transition in the unsubstituted CP ring. The signal at 259 nm may be linked to  $n \rightarrow \sigma^*$  transition in C–OH due to better electron donating effect of ferrocenyl group. The peak at 296 nm corresponding to  $\pi \rightarrow \pi^*$  transition is attributed to more conjugated *para* cyclopentadienyl benzoate chromophore. The less intense band at 364 nm can be linked to  $n \rightarrow \pi^*$  transition of carbonyl group and the least intense band at 460 nm may be due to  $d-d$  transition. The spectra of **2** also registered five peaks like **5** but with different position and height. However, the spectrum of **4** recorded four (two intense and two broad) peaks. The more intense peak at 234 nm can be corresponded to  $\pi \rightarrow \pi^*$  transition in both  $C_p$  rings. The absence of peak at 259 nm in case of meta directing groups may be due to the weak electron donating effect of ferrocenyl group to excite  $n \rightarrow \sigma^*$  transition. The peak at 280 nm can presumably be associated with  $\pi \rightarrow \pi^*$  transition in less conjugated cyclopentadienyl benzoate group. The two broad bands at longer wavelengths are attributable to  $n \rightarrow \pi^*$  and  $d-d$  transition in carbonyl group and iron respectively. The electronic spectral responses of **1** and **3** were found in good agreement with **4**. The differences in the absorption spectra of **5** and **4** demonstrate

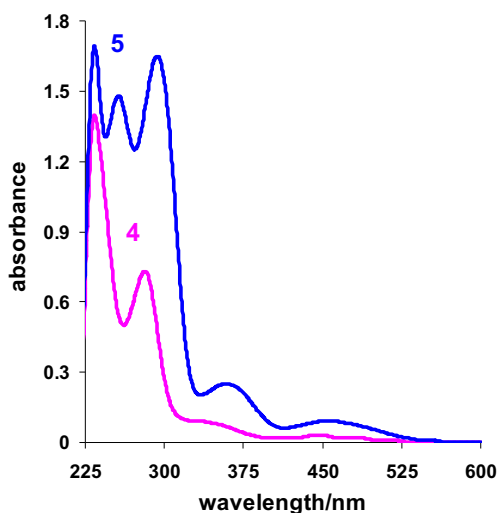


Fig. 5. UV–Vis spectra of 45  $\mu\text{M}$  **4** and **5**.

that the UV–Vis signature can be modulated by the carboxyl group attached at *para* and *meta* position.

The UV–Vis spectra of 10–50  $\mu\text{M}$  **5** can be seen in Fig. 4 of supplementary materials. The absorption coefficients of all peaks in the spectra of *para* and *meta* ferrocenyl derivatives were evaluated. The *para* derivatives showed four bands in UV and one in visible region while the *meta* derivatives registered three envelopes in the UV and one in the visible part of the spectrum. The absorption coefficients varied from  $3.84 \times 10^4$  to  $6.60 \times 10^2 \text{ M}^{-1}\text{cm}^{-1}$ . The values are in close agreement with those reported for ferrocenyl chalcones [43]. The greater extinction coefficient of **5** ( $1.87 \times 10^3 \text{ M}^{-1}\text{cm}^{-1}$ ) at 460 nm as compared to **4** ( $6.90 \times 10^2 \text{ M}^{-1}\text{cm}^{-1}$ ) at 451 nm is attributed to the more effective electron withdrawing ability of  $-\text{COOH}$  at *para* position thus making the cyclopentadienyl ring to act as a weak donor. The poor donating group capable of causing lower splitting of  $d-d$  orbitals of iron will result in higher probability of electronic transition at longer wavelength. The interactions of organoantimony ferrocenyl benzoates with DNA were examined by UV–Visible spectroscopy in order to get some information about their mode of interaction and binding strength. UV–Vis absorption spectrometry is the most frequently employed method for the detection of drug–DNA interaction and assessment of binding mode due to its good sensitivity, simplicity, reproducibility and versatility [45,46]. The peak at 235 nm (Fig. 6), exhibiting blue shift in the presence of increasing concentration of DNA can be attributed to the electrostatic interaction of the partial positive iron of **3** with the negatively charged oxygen of DNA. While the peak at 279 nm exhibiting hypochromism and slight red shift is indicative of groove binding according to the criteria suggested for the mode of interaction by the previous investigators [46]. Hence, complex **3** interacts with DNA by mixed binding mode (electrostatic and groove binding) due to different interacting moieties. The hypochromic effect is thought to be due to the interaction between the electronic states of the binding chromophore and those of the DNA bases [47]. It is expected that the strength of this electronic interaction would decrease as the cube of the distance of separation between the chromophore and the DNA bases [48]. So, the obviously large hypochromism observed in our experiments suggested the close proximity of the chromophore of **3** to the DNA bases. At the closest approach to DNA, the  $\pi^*$  orbital of the binding moiety of **3** could couple with  $\pi$  orbital of purine or pyrimidine. The coupling  $\pi^*$  orbital may get partially filled by electrons, thus

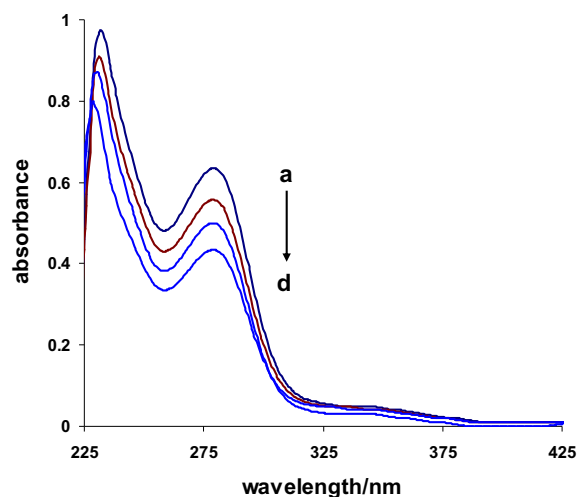


Fig. 6. UV–Vis spectra of 25  $\mu\text{M}$  **3** in the (a) absence and (b–d) presence of 4.0, 7.0 and 20.0  $\mu\text{M}$  DNA.

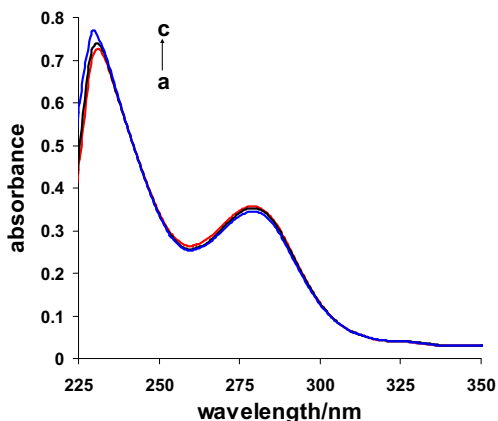


Fig. 7. UV–Vis spectra of 25  $\mu\text{M}$  **1** in the (a) absence and (b–c) presence of 3.0 and 7.0  $\mu\text{M}$  DNA.

decreasing the transition probabilities, and hence result in hypochromism [49,50].

The UV–Vis spectral characteristics of **4** with DNA were very much similar to that of **3**. However, the interesting observation for **1** in the presence of DNA was the increase in absorbance (hyperchromism) accompanied with very slight blue shift (Fig. 7). The observed spectral effects can be explained by the electrostatic interaction of **1** with the negatively charged oxygen causing structural damage of DNA in the time domain of the experiment. F. Arjmand and S. Shi have also reported that hyperchromic effect arises mainly due to the binding of drug with DNA *via* electrostatic attraction thereby causing a contraction and overall damage to the secondary structure of DNA [51,52].

For the **2**, stronger interaction with DNA was observed as shown in Fig. 8. The peak at 227 nm due to  $\pi \rightarrow \pi^*$  transition in the CP ring after the addition of DNA got red shifted and almost disappeared indicating drastic structural changes at this chromophore. The substantial bathochromic shift can be attributed to the intercalation of the planar part of **2** in to the double stranded DNA and the diminution of the intensity can presumably be due to the shielding of the ferrocenyl moiety by its probable fitting into the grooves of DNA. Kohji et al. [53], have documented that the distance of approximately 3.3 Å, between the two Cp rings is close to the typical distance of two aromatic rings in parallel-stacking geometry. Because pyrrole-imidazole amides (PIA) can bind to the DNA

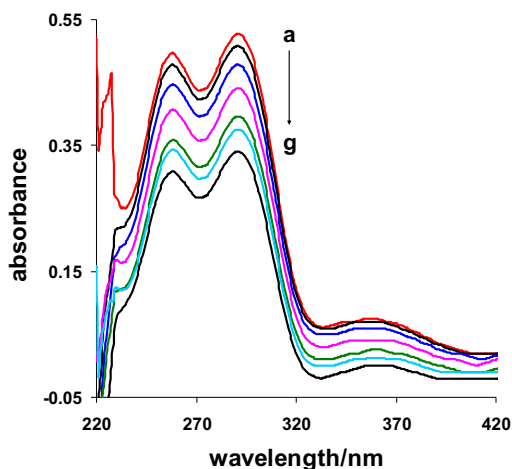


Fig. 8. UV–Vis spectra of 25  $\mu\text{M}$  **2** in the (a) absence and (b–g) presence of 2.0, 3.0, 4.0, 5.0, 6.0 and 7.0  $\mu\text{M}$  DNA.

groove as a stacked dimer, so it is expected that the ferrocene moiety of **2** can fit the groove when it binds to the DNA duplex in a conformation similar to that of the conventional PIA dimers [53]. The suggested mixed binding mode (intercalation and groove binding) will unwind the DNA helix at the interaction sites which may lead to perturbation in its normal functioning that may culminate in the death of cancerous cell.

The absence of red shift in the UV–Vis spectra of **5** after the addition of DNA (see Fig. 5 of supplementary materials) ruled out the involvement of intercalation. The reason is not far to seek. The planar part being sandwiched in two ferrocenyl groups may not approach to the stacked base pairs. Hence, the UV–Vis spectra of **5** evidenced slight electrostatic and dominant groove binding mode. Since absorbance varied in the presence of dsDNA, so based on variation in absorption maxima the binding constant “*K*” of drug–DNA complexation was determined according to Wolfe–Shimer equation [54]:

$$\frac{[\text{DNA}]}{\varepsilon_A - \varepsilon_F} = \frac{[\text{DNA}]}{\varepsilon_B - \varepsilon_F} + \frac{1}{K_f(\varepsilon_B - \varepsilon_F)} \quad (5)$$

where  $\varepsilon_A$ ,  $\varepsilon_F$  and  $\varepsilon_B$  correspond to  $A_{\text{observed}}/[M]$ , the extinction coefficient of the free drug, and the extinction coefficient of the drug in the fully bound form, respectively. The binding constant was obtained from the slope to intercept ratio of the plot of  $[\text{DNA}]/(\varepsilon_A - \varepsilon_F)$  versus  $[\text{DNA}]$ .

The binding constant varied in the same sequence as revealed by CV results. The highest *K* of **2** suggested its greater DNA binding affinity than other ferrocenes.

#### 4. Conclusion

Ferrocene–antimony complexes with tunable redox and spectroscopic properties were synthesized and characterized by electrochemical and spectroscopic techniques with the aim of investigating their potential anticancer activity. All the compounds were found to follow one electron reversible redox process in a diffusion controlled manner at a potential higher than simple ferrocene. Hyperchromism, hypochromism, cathodic and anodic peak potential shifts suggested OFBs to interact with DNA by different modes due to variation in configuration. The binding constant was found to vary in the sequence:  $K_2 > K_1 > K_3 > K_4 > K_5$ . The present study is expected to provide deep insights about the understanding of unexplored mechanism by which such compounds exert their biochemical action. The solid phase structure of the complex **5** adopts an approximate trigonal bipyramidal Sb coordination environment with unidentate carboxylate ligands in the axial positions at *trans* orientation with respect to ferrocenyl moiety.

#### Acknowledgements

Dr. M. Khawar Rauf is thankful to Quaid-i-Azam University Islamabad, Pakistan for Post-doctoral Fellowship and the grant of funds to carry out this research work. Authors also acknowledge the financial support from Higher Education Commission of Pakistan.

#### Appendix A. Supplementary material

Crystallographic data (excluding structure factors) for the structures reported in this paper have been deposited to the Cambridge Crystallographic Data Centre as supplementary publication no. CCDC-881520 for **5**. Copies of available materials can be obtained, free of charge, on application to the director, CCDC, 12

Union Road, Cambridge CB21EZ, UK, (Fax: +44-(0)-1223-336033 or e-mail: deposit@ccdc.cam.ac.uk).

## Appendix B. Supplementary material

Supplementary data associated with this article can be found in the online version, at <http://dx.doi.org/10.1016/j.jorganchem.2012.07.028>.

## References

- [1] (a) L. Yu, Y.-Q. Ma, R.-C. Liu, G.-C. Wang, J.-S. Li, G.-H. Du, J.-J. Hu, *Polyhedron* 23 (2004) 823–829;  
(b) W.J. Lile, R.C. Menzies, *J. Chem. Soc.* (1950) 617–621.
- [2] R.-C. Liu, Y.-Q. Ma, L. Yu, J.-S. Li, J.-R. Cui, R.-Q. Wang, *Appl. Organomet. Chem.* 17 (2003) 662–668.
- [3] J.-S. Li, R.-C. Liu, X.-B. Chi, G.-C. Wang, Q.-S. Guo, *Inorg. Chim. Acta* 357 (2004) 2176–2180.
- [4] H. Yin, L. Quan, L. Li, *Inorg. Chem. Commun.* 11 (2008) 1121–1124.
- [5] P. Stepnicka (Ed.), *Ferrocenes: Ligands, Materials and Biomolecules*, John Wiley & Sons, March 25, 2008.
- [6] C. Ornelas, *New J. Chem.* 35 (2011) 1973–1985.
- [7] C. Roux, C. Biot, *Future Med. Chem.* 4 (6) (2012) 783–797.
- [8] P. Meunier, I. Ouattara, B. Gautheron, J. Tirouflet, D. Camboli, J. Besancon, *Eur. J. Med. Chem.* 26 (1991) 351–362.
- [9] S. Top, J. Tang, A. Vessieres, D. Carrez, C. Provot, G. Jaouen, *Chem. Commun.* (1996) 955–956.
- [10] Z. Dori, D. Gershon, Y. Scharf, F.R.F. Demande, 2,598,616 (Cl. A61K31/12), 20 Nov. 1987, US Appl. 862,804, 13th May 1986, p. 13.
- [11] D. Osella, M. Ferrali, P. Zanella, F. Laschi, M. Fontani, C. Nervi, G. Cavigiolo, *Inorg. Chim. Acta* 306 (2000) 42–48.
- [12] L.V. Snegur, V.N. Babin, A.A. Simenel, Y.S. Nekrasov, L.A. Ostrovskaya, N.S. Sergeeva, *Russ. Chem. Bull.* 59 (2010) 2167–2178.
- [13] C. Biot, N. Francois, L. Maciejewski, J. Brocard, D. Poulain, *Bioorg. Med. Chem. Lett.* 10 (2000) 839–841.
- [14] T. Itoh, S. Shirakami, N. Ishida, Y. Yamashita, T. Yoshida, H.-S. Kim, Y. Wataya, *Bioorg. Med. Chem. Lett.* 10 (2000) 1657–1659.
- [15] J. Huangxian, Y. Baofen, G. Jiayin, *Sensors* 4 (2004) 71–83.
- [16] H. Schmidt, F.M. Peter, *Advances in the Therapeutics of Antimony*, Thieme Verlag, Leipzig, 1938.
- [17] T.D. Luckey, B. Venugopal, *Metal Toxicity in Mammals*, vol. 2, Plenum Press, New York, 1997.
- [18] P. Aggarwal, R. Handa, S. Singh, J.P. Wali, *Ind. J. Pediatr.* 66 (1999) 63–71.
- [19] P. Sharma, D. Perez, A. Cabrera, N. Rosas, J.L. Arias, *Acta Pharmacol. Sin* 29 (2008) 881–890.
- [20] J. Duffin, B.G. Campling, *J. Hist. Med.* 57 (2002) 61–78.
- [21] T.-L. Yi, M.K. Pathak, D.J. Lindner, M.E. Ketterer, C. Farver, E.C. Borden, *J. Immunol.* 169 (2002) 5978–5985.
- [22] C.-T. Yeh, D.-R. Hwang, H.-Y. Lai, J.-T.A. Hsu, *Biochem. Biophys. Res. Commun.* 310 (2003) 537–541.
- [23] M.J. Warning, *J. Mol. Biol.* 13 (1965) 269–282.
- [24] J.B. Chaires, N. Dattagupta, D.M. Crothers, *Biochemistry* 21 (1982) 3933–3940.
- [25] M.R. Arkin, E.D.A. Stemp, C. Turro, N.J. Turro, J.K. Barton, *J. Am. Chem. Soc.* 118 (1996) 2267–2274.
- [26] W. Zhong, J.H. Yu, Y. Liang, *Spectrochim. Acta Part A* 59 (2003) 1281.
- [27] Z. Rehman, A. Shah, N. Muhammad, S. Ali, R. Qureshi, I.S. Butler, *J. Organomet. Chem.* 694 (2009) 1998–2004.
- [28] Z. Rehman, A. Shah, N. Muhammad, S. Ali, R. Qureshi, I.S. Butler, *Eur. J. Med. Chem.* 44 (2009) 3986–3993.
- [29] J. Grau, V. Noe, C. Ciudad, M.J. Prieto, M. Font-Bardia, T. Calvet, V. Moreno, *J. Inorg. Biochem.* 109 (2012) 72–81.
- [30] M.C. Gimeno, H. Goitia, A. Laguna, M.E. Luque, M.D. Villacampa, C. Sepúlveda, M. Meireles, *J. Inorg. Biochem.* 105 (2011) 1373–1382.
- [31] G.M. Sheldrick, *Acta Cryst. A* 64 (2008) 112–122.
- [32] K.-Q. Zhao, P. Hu, H.-B. Xu, *Molecules* 6 (2001) M246.
- [33] M. Aslanoglu, *Anal. Sci.* 22 (2006) 439–445.
- [34] N. Li, Y. Ma, C. Yang, L. Guo, X. Yan, *Biophys. Chem.* 116 (2005) 199–205.
- [35] X. Chu, G.-L. Shen, J.-H. Jian, T.-F. Kang, B. Xiong, R.-Q. Yu, *Anal. Chim. Acta* 373 (1998) 29–38.
- [36] T.W. Welch, H.H. Thorp, *J. Phys. Chem.* 100 (1996) 13829–13836.
- [37] M.T. Carter, M. Rodriguez, A.J. Bard, *J. Am. Chem. Soc.* 111 (1989) 8901–8911.
- [38] Q. Feng, N.-Q. Li, Y.-Y. Jiang, *Anal. Chim. Acta* 344 (1997) 97–114.
- [39] A. Shah, M. Zaheer, R. Qureshi, Z. Akhtar, M. Faizan, *Spectrochim. Acta A* 75 (2010) 1082–1087.
- [40] C.M.A. Brett, A.M.O. Brett, *Electrochemistry Principles, Methods and Applications*, Oxford University Press, UK, 1993.
- [41] A. Shah, R. Qureshi, M.A. Khan, R.A. Khera, F.L. Ansari, *J. Braz. Chem. Soc.* 21 (2010) 447–451.
- [42] A. Shah, R. Qureshi, M.A. Khan, F.L. Ansari, S. Ahmed, *Bull. Chem. Soc. Jpn.* 82 (2009) 453–457.
- [43] R.A. Cardona, K. Hernández, L.E. Pedró, M.R. Otaño, I. Montes, A.R. Guadalupéz, *J. Electrochem. Soc.* 157 (2010) F104–F110.
- [44] A. Shah, V.C. Deculescu, R. Qureshi, A.M.O. Brett, *Bioelectrochemistry* 77 (2010) 145–150.
- [45] M. Kožurková, D. Sabolová, L. Janovec, J. Mikeš, J. Koval, J. Ungvarský, M. Štefanišínová, P. Fedorocko, P.I. Kristian, *Bioorg. Med. Chem.* 16 (2008) 3976–3984.
- [46] (a) X.-L. Zhao, M.-J. Han, A.-G. Zhang, K.-Z. Wang, *J. Inorg. Biochem.* 107 (2012) 104–110;  
(b) A. Vessières, C. Corbet, J.M. Heldt, N. Lories, N. Jouy, I. Laíos, G. Leclercq, G. Jaouen, R.-A. Toillon, *J. Inorg. Biochem.* 104 (2010) 503–511.
- [47] R. Fukuda, S. Takenaka, M. Takagi, *J. Chem. Soc. Chem. Commun.* (1990) 1028–1030.
- [48] C. Cantor, P.R. Schimmel, *Biophysical Chemistry*, W.H. Freeman, San Francisco, 1980.
- [49] C.-C. Ju, A.-G. Zhang, C.-L. Yuan, X.-L. Zhao, K.-Z. Wang, *J. Inorg. Biochem.* 105 (2011) 435–443.
- [50] V. Gonzalez-Ruiz, A.I. Olives, M.A. Martin, P. Ribelles, M.T. Ramos, J.C. Menendez, *Biomedical Engineering, Trends, Research and Technologies, InTech, India*, 2011, ISBN 978-953-307-514-3, pp. 65–90.
- [51] S. Shi, J. Liu, J. Li, K.-C. Zheng, X.-M. Huang, C.-P. Tan, L.-M. Chen, L.N. Ji, *J. Inorg. Biochem.* 100 (2006) 385–395.
- [52] F. Arjmand, F. Sayeed, *J. Mol. Struct.* 965 (2010) 14–22.
- [53] K. Seio, M. Mizuta, T. Terada, M. Sekine, *J. Org. Chem.* 70 (2005) 10311–10322.
- [54] A. Wolfe, G.H. Shimer, T. Meehan, *Biochemistry* 26 (1987) 6392–6396.